J Appl Physiol 109: 1619–1627, 2010.
First published September 30, 2010; doi:10.1152/japplphysiol.01356.2009.

Effect of blood pressure on vascular hemodynamics in acute tachycardia

Hai Zheng,[1]* Yunlong Huo,[1]* Mark Svendsen,[4] and Ghassan S. Kassab[1,2,3,4]

Departments of [1]Biomedical Engineering, [2]Surgery, and [3]Cellular and Integrative Physiology, Indiana University Purdue University Indianapolis, Indianapolis; and [4]Weldon School of Biomedical Engineering, Purdue University, West Lafayette, Indiana

Submitted 7 December 2009; accepted in final form 26 September 2010

Zheng H, Huo Y, Svendsen M, Kassab GS. Effect of blood pressure on vascular hemodynamics in acute tachycardia. *J Appl Physiol* 109: 1619–1627, 2010. First published September 30, 2010; doi:10.1152/japplphysiol.01356.2009.—Paroxysmal supraventricular tachycardia is accompanied by hypotension, which can affect vascular hemodynamics. Here, we hypothesized that a fall in blood flow as a result of hypotension has a larger effect on hemodynamics in medium-sized peripheral arteries compared with increased pulsatility in rapid pacing. To test this hypothesis, we experimentally and theoretically investigated hemodynamic changes in femoral, carotid, and subclavian arteries at heart rates of 95–170 beats/min after acute pacing. The arterial pressure, blood flow, and other hemodynamic parameters remained statistically unchanged for heart rates ≤135 beats/min. Systemic pressure and flow velocities, however, showed an abrupt decrease, resulting in larger alteration of hemodynamic parameters for heart rates ≥155 beats/min after pacing (initial period) and then recovered close to baseline after several minutes of pacing (recovery period). During the initial period, the pressure dropped from 88 mmHg (baseline) to 44 mmHg, and the flow velocity decreased to about one-third of baseline at heart rate of 170 beats/min. A hemodynamic analysis showed a velocity profile with a near-wall retrograde flow or a fully reversed flow during the initial period, which vanished at the recovery period. It was concluded that the initial fall of blood flow due to pressure drop led to transient flow reversal and negative wall shear stress because this phenomena was not observed at the recovery period. This study underscores the significant effects of hypotension on vascular hemodynamics, which may have relevance to physiology and chronic pathophysiology in paroxysmal supraventricular tachycardia.

hypotension; flow reversal; wall shear stress

MORE THAN 1% OF THE US POPULATION is affected by supraventricular tachycardia (SVT) (4). The paroxysmal SVT (PSVT) refers to a SVT that begins and ends abruptly (28). The PSVT generally reduces cardiac output due to incomplete filling and incoordinate contraction at its onset, which results in hypotension (21). The typical symptoms of PSVT include dizziness, syncope (in serious cases), and limb numbness (20, 26), which are believed to be associated with hypotension (1). The abnormal vasomotor response to the hemodynamic stress related to hypotension is an important mechanism for syncope and numbness (20) in PSVT, and the ischemia/hypoxia to brain and limbs are one potential cause. Although the reflex effects of PSVT on autonomic tone have been widely investigated (29), the relation between PSVT and vascular hemodynamics in respective arteries (carotid for brain and subclavian and femoral for extremities) remains relatively unknown.

The objective of the present study is to investigate the changes of vascular hemodynamics as a result of systemic hypotension in acute tachycardia. A fall in blood flow as a result of hypotension is hypothesized to have a larger effect on hemodynamics in femoral, carotid, and subclavian arteries compared with increased pulsatility in rapid pacing. Consequently, we investigated hemodynamic changes in these arteries at heart rates of 95–170 beats/min after acute pacing experimentally and analytically. The former was done through simultaneous measurements of in vivo pressure, blood flow, and cross-sectional area (CSA) in femoral, carotid, and subclavian arteries of swine. The latter was completed through analytic fluid dynamics, based on measured geometry (diameters and lengths) and boundary conditions (flow) and laws of mechanics, to determine the velocity profile, wall shear stress (WSS), and oscillatory shear index (OSI).

EXPERIMENTAL METHODS

Animal Preparation

Studies were performed on eight domestic swine weighing 77 ± 8 kg. The animal preparation was similar to that described by Kassab et al. (17, 18). The animal experiments were performed in accordance with the guidelines of the Institute of Laboratory Animal Research Guide, Public Health Service Policy, Animal Welfare Act, and an approved Indiana University School of Medicine Institutional Animal Care and Use Committee protocol.

Briefly, surgical anesthesia was induced with TKX (Telaxol 500 mg, ketamine 250 mg, xylazine 250 mg) and maintained with 2% isoflurane. The animal was intubated and ventilated with room air and oxygen by a respiratory pump. A side branch from the left jugular vein was dissected and cannulated with a 7Fr sheath for administration of drugs (e.g., heparin, lidocaine, levophed, and saline). The right femoral artery was cannulated with a 7Fr sheath and connected to a pressure transducer (Summit Disposable Pressure Transducer, Baxter Healthcare; error of ±2% at full scale) for monitoring arterial blood pressure. In two animals, the left carotid artery was cannulated with a 7Fr sheath for pressure measurements.

The right jugular vein was exposed and cannulated with a 9Fr sheath for the advancement of the pacing lead into the right atrium. The pacing lead (Medtronic 5568, Medtronic) was screwed into the wall of the right atrium and connected to a pacemaker (Medtronic Enpulse E2DR01), which was placed into a subcutaneous pocket. The femoral, carotid, and subclavian arteries were dissected. Perivascular flow probes (Transonic Systems; relative error of ±2% at full scale) were mounted on these arteries to measure the volumetric flow rate. Flow and pressure were continuously recorded using a Biopac MP 150 data-acquisition system (Biopac Systems). The CSA of arteries was determined using ultrasound (Philips IE33 ultrasound system with a L15–7 probe).

Measurement of Pulsatile Flow and CSA

The heart rate was paced to 95, 115, 135, 155, and 170 beats/min (basal heart rate of ~90 beats/min), and measurements were made

* H. Zheng and Y. Huo contributed equally to this work.

Address for reprint requests and other correspondence: G. S. Kassab, Dept. of Biomedical Engineering, Indiana Univ. Purdue Univ. Indianapolis, Indianapolis, IN 46202 (e-mail: gkassab@iupui.edu).

8750-7587/10 Copyright © 2010 the American Physiological Society

Downloaded from journals.physiology.org/journal/jappl (073.144.208.122) on April 15, 2022.

immediately after rapid pacing at each heart rate. The animal was allowed to recover to baseline between consecutive rapid pacing sessions. Electrocardiography signals were used to monitor the heart rate. At each heart rate, the dynamic change of CSA over several cardiac cycles was monitored by ultrasound. We determined the CSA of these arteries at the same instances in the cardiac cycle (the time interval between two consecutive instances is constant) and then averaged them over time. Pulsatile volumetric flow rates of femoral, carotid, and subclavian arteries were recorded continuously for ~10 min using perivascular flow probes under each heart rate after pacing. The femoral arterial pressure was measured by a pressure transducer during the entire procedure. The carotid arterial pressure was monitored, and the mean value was found to be ~3 mmHg higher than the femoral pressure in the supine position.

Data Analysis

Flow velocity waves were calculated as volumetric flow waves divided by CSA. The pressure, volumetric flow rate, and flow velocity waves were averaged over a cardiac cycle to yield the time-averaged values at each heart rate. The vessel diameter was obtained from the measured CSA, and vascular resistance was determined as the ratio of the time-averaged pressure to the volumetric flow rate. The mean ± SD of various hemodynamic parameters was determined for the eight animals. A two-way ANOVA (SigmaStat 3.5) was used to compare hemodynamic parameters between baseline and initial period at each heart rate and between different arteries (i.e., femoral vs. carotid, carotid vs. subclavian, and subclavian vs. femoral), as shown in Table 1, where $P < 0.05$ represented statistically significant differences. The pressure and flow waveforms obtained from the eight animals were similar and showed the same trend as the heart rate increased. Therefore, we present data from a representative animal in Figs. 1–4.

Mathematical Model

Hemodynamic parameters. Reynolds (Re) and Womersley (α) numbers are important hemodynamic parameters that characterize pulsatile blood flows in arteries (e.g., transition from laminar to turbulence, etc.). They are defined, respectively, as follows:

$$\mathrm{Re} = \frac{\rho V_{\mathrm{mean}} \cdot D}{\mu} \tag{1}$$

$$\alpha = \frac{D}{2}\sqrt{\frac{\omega\rho}{\mu}} \tag{2}$$

where V_{mean} is time-averaged velocity, D is the diameter of artery, ω is the angular frequency of heart rate, ρ is the blood mass density, and μ is the dynamic viscosity. *Equation 1* is the ratio of convective inertia to viscous forces, whereas *Eq. 2* is the ratio of transient inertia to viscous forces.

Analytic solution for pulsatile flow pattern and WSS. The details of mathematical derivations are shown in the APPENDIX. Briefly, if the blood vessel is assumed to be cylindrical, straight, and fully long, the equation for the pulsatile flow velocity profile across the lumen, $u(r,t)$, is given as:

$$u(r,t) = \mathrm{REAL}\left[\frac{2Q(x,0)\left(R^2 - r^2\right)}{\pi R^4} + \sum_{\omega=1}^{\infty} \frac{\dfrac{Q(r,\omega)}{\pi R^2} \cdot \left[1 - \dfrac{J_0(\Lambda r/R)}{J_0(\Lambda)}\right]}{1 - \dfrac{2J_1(\Lambda)}{\Lambda J_0(\Lambda)}} e^{i\omega t}\right] \tag{3}$$

where t is time; r is the radial coordinate; R is the radius of artery; $\Lambda^2 = i^3\alpha^2$, $q(x,t) = Q(x,\omega)e^{i\omega t}$ is the volumetric flow wave determined by experimental measurements; ω are angular frequencies after Fourier Transformation; J_0 is a Bessel function of zero order and first kind; and J_1 is a Bessel function of first order and first kind. Accordingly, WSS and OSI for pulsatile blood flow, $\tau(r,t)$ and OSI, respectively, can be written as:

Table 1. *Hemodynamic parameters at initial period in rapid pacing*

Heart Rate, beats/min	Pressure, mmHg	Flow Rate, ml/min	Flow Velocity, cm/s	Diameter, mm	Resistance, mmHg·min·ml^{-1}	Re	α
				Femoral artery			
95	88 ± 7	196 ± 25†‡	32 ± 14	3.97 ± 1.45‡	0.44 ± 0.04†‡	297 ± 80†‡	3.22 ± 1.18‡
115	87 ± 6	191 ± 38†‡	28 ± 10	4.02 ± 1.09‡	0.47 ± 0.12†‡	276 ± 62†‡	3.59 ± 0.98‡
135	81 ± 9	163 ± 34†‡	22 ± 7*	4.08 ± 1.01‡	0.49 ± 0.09†‡	230 ± 42†‡	3.95 ± 0.98*‡
155	58 ± 16*	106 ± 44*†‡	14 ± 6*	4.18 ± 0.85‡	0.63 ± 0.13†‡	144 ± 52*†‡	4.33 ± 0.89*‡
170	44 ± 16*	59 ± 22*†‡	8 ± 3*	4.22 ± 0.70‡	0.73 ± 0.15*†‡	81 ± 32*†‡	4.58 ± 0.77*‡
				Carotid artery			
95		339 ± 91†	39 ± 13	4.32 ± 0.65	0.29 ± 0.08†	443 ± 115†	3.51 ± 0.54
115		343 ± 61†	36 ± 3	4.46 ± 0.36	0.28 ± 0.08†	430 ± 48†	3.99 ± 0.32
135		318 ± 39†	34 ± 3*	4.48 ± 0.18§	0.27 ± 0.06†	399 ± 40†	4.34 ± 0.17*
155		227 ± 92*†	23 ± 7*	4.53 ± 0.25§	0.30 ± 0.04†	278 ± 96*†	4.69 ± 0.26*
170		146 ± 66*†	15 ± 5*	4.52 ± 0.56§	0.36 ± 0.08†	178 ± 68*†	4.93 ± 0.61*
				Subclavian artery			
95		422 ± 141‡	34 ± 11	5.18 ± 0.98‡	0.23 ± 0.09‡	459 ± 143‡	4.21 ± 0.79‡
115		421 ± 145‡	32 ± 12	5.36 ± 0.95‡	0.22 ± 0.09‡	444 ± 150‡	4.79 ± 0.85‡
135		349 ± 141‡	24 ± 8*	5.50 ± 0.81§‡	0.25 ± 0.12‡	357 ± 127‡	5.33 ± 0.78*‡
155		310 ± 112*‡	21 ± 4*	5.56 ± 0.55§‡	0.27 ± 0.07‡	308 ± 79*‡	5.77 ± 0.57*‡
170		148 ± 43*‡	11 ± 2*	5.39 ± 0.44§‡	0.31 ± 0.07‡	153 ± 34*‡	5.85 ± 0.47*‡

Values are means ± SD. The mean values were averaged over eight animals. Resistance was defined as the ratio of pressure to flow rate. Re and α refer to Reynolds and Womersley numbers, respectively. *Statistical significance ($P < 0.05$, determined by the Holm-Sidak method in a two-way ANOVA) of those hemodynamic parameters between control and initial period under various heart rates. Statistical significance ($P < 0.05$, determined by the Holm-Sidak method in a two-way ANOVA) of those hemodynamic parameters for †femoral vs. carotid, §carotid vs. subclavian, and ‡subclavian vs. femoral.

Downloaded from journals.physiology.org/journal/jappl (073.144.208.122) on April 15, 2022.

$$\tau(r,t) = \mathrm{REAL}\left[\frac{4\mu}{\pi R^3}Q(r,0) - \sum_{\omega=1}^{\infty}\frac{\dfrac{\mu Q(r,\omega)}{\pi R^3}\cdot\dfrac{\Lambda J_1(\Lambda)}{J_0(\Lambda)}}{1-\dfrac{2J_1(\Lambda)}{\Lambda J_0(\Lambda)}}e^{i\omega t}\right] \quad (4)$$

$$\mathrm{OSI} = \frac{1}{2}\left[1 - \frac{\left|\dfrac{1}{T}\int_0^T \tau(R,t)\right|}{\dfrac{1}{T}\int_0^T \left|\tau(R,t)\right|}\right] \quad (5)$$

where T is the period of a cardiac cycle. *Equations 1–5* were used to determine hemodynamic parameters and flow velocity profiles for pulsatile blood flows when volumetric flow waves were measured in peripheral arteries at various heart rates. The viscosity (μ) and density (ρ) were assumed to be 4.5 cP and 1.06 g/cm^3, respectively.

RESULTS

Figure 1, *A–C*, shows pressure waves in a representative femoral artery at baseline (~90 beats/min) and initial and recovery periods, respectively, at the heart rate of 155 beats/min. Compared with baseline (Fig. 1*A*), the time-averaged pressure dropped immediately after pacing (Fig. 1*B*), and then recovered close to baseline in about 3 min of pacing (Fig. 1*C*). Accordingly, Fig. 2, *A–C*, *D–F*, and *G–I*, shows volumetric flow waves at baseline and initial and recovery periods in femoral, carotid, and subclavian arteries, respectively. Similar to the systemic pressure, the time-averaged flows in those arteries declined during the initial period and then returned close to baseline during the recovery period.

Table 1 shows hemodynamic parameters (mean ± SD) in femoral, carotid, and subclavian arteries during the initial period after rapid pacing, where mean values were averaged over eight animals. Table 2 shows the *P* values for the effect of heart rate, artery type, and interaction between heart rate and artery type, which are consistent with the statistical analysis determined by the Holm-Sidak method in a two-way ANOVA, as shown in Table 1. Systemic pressure, flow rate, and velocity decreased with pacing, which were statistically different from baseline with heart rates ≥155 beats/min. Although the diameter and resistance of these arteries increased, the difference was not statistically significant, except for the vascular resistance in the femoral artery, which increased significantly at heart rate of 170 beats/min. The Reynolds and Womersley numbers were significantly decreased and increased, respectively, at higher heart rates (≥155 beats/min), as shown in Table 1. A statistical comparison shows that the hemodynamic parameters in femoral artery are significantly different from those in subclavian artery. There is no statistically significant interaction between heart rate and artery type.

Figure 3, *A–C*, shows normalized flow velocity profiles as a function of normalized radial position in femoral artery at time instances with maximal and minimal flow rates over a cardiac cycle (peak and trough flows, respectively) at baseline and initial and recovery periods, respectively. Fig. 3, *D–F* and *G–I*, shows normalized flow velocity profiles in carotid and subclavian arteries, respectively, in correspondence with Fig. 3, *A–C*. The flow velocity profiles at baseline were similar to those at the recovery period, while there were stronger flow reversals in trough flow at the initial period.

Figure 4, *A–I*, shows WSS waves in femoral, carotid, and subclavian arteries at baseline and initial and recovery periods in correspondence to Fig. 2, *A–I*. The time-averaged WSS dropped immediately after the onset of atrial pacing with a heart rate of 155 beats/min, and the minimal value fell below zero in all three arteries. The OSI computed by *Eq. 5* has a value of 0.11, 0.04, and 0.27 in femoral, carotid, and subclavian arteries, respectively, at the initial period. The values of OSI was equal to zero in femoral and carotid arteries and 0.06 in subclavian artery at baseline. There was no statistical difference in time-averaged WSS and OSI between the baseline and recovery period. The difference between baseline and initial pacing was quite apparent.

DISCUSSION

The in vivo measurements of pressure and flow waves and CSAs were made in femoral, carotid, and subclavian arteries of eight swine at heart rates of 95–170 beats/min after rapid atrial pacing. The following three major findings were observed: *1*) hemodynamic parameters (i.e., arterial pressure, blood flow, resistance, and Reynolds and Womersley number) remained relatively unchanged for heart rates ≤ 135 beats/min; *2*) most of these parameters changed significantly during the initial period after the heart was paced with rates ≥ 155 beats/min,

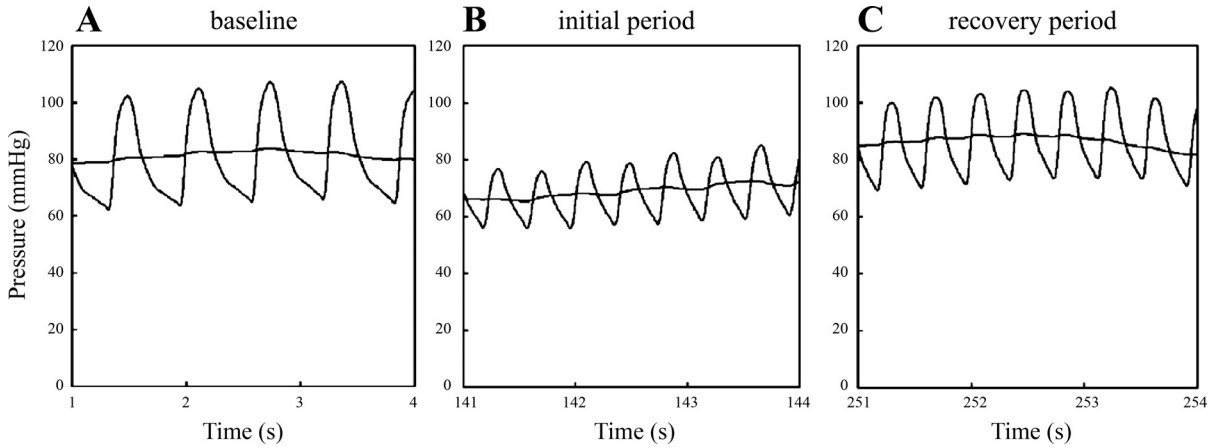

Fig. 1. Pressure waves (unit: mmHg) at baseline (~90 beats/min; *A*), initial period (*B*), and recovery period (*C*) after the heart rate of a representative pig is paced to 155 beats/min. The horizontal solid line represents the time-averaged pressure over a cardiac cycle.

Downloaded from journals.physiology.org/journal/jappl (073.144.208.122) on April 15, 2022.

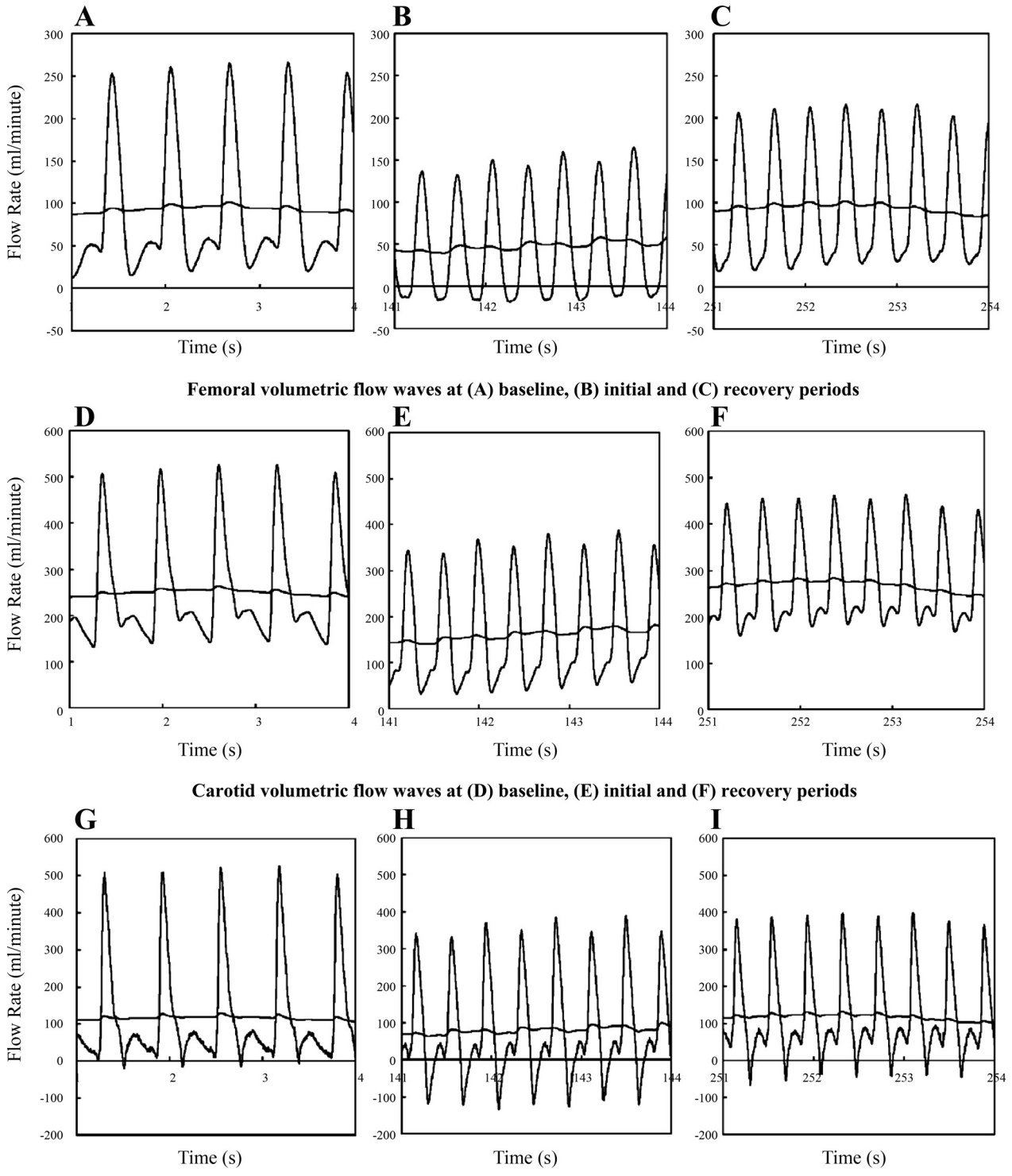

Fig. 2. Volumetric flow waves (unit: ml/min) in femoral artery at baseline (~90 beats/min; *A*), initial period (*B*), and recovery period (*C*) after the heart rate of a pig is paced to 155 beats/min, corresponding to Fig. 1, *A–C*. Volumetric flow waves are shown in carotid artery (*D–F*) and subclavian artery (*G–I*), in correspondence with *A–C*. The horizontal solid line represents the time-averaged volumetric flow rate over a cardiac cycle.

which caused a stronger flow reversal, lower WSS, and higher OSI, while the CSA and resistance remained relatively unchanged; and *3*) these altered parameters, as well as the flow pattern, WSS, and OSI, returned close to baseline during the recovery period.

The rapid pacing led to a significant decrease of time-averaged pressure and flow in these arteries during the initial period with heart rates ≥ 155 beats/min, which recovered close to baseline in ~3 min. The abrupt shortening of diastole and reduction of ventricular filling due to tachycardia resulted in a

Downloaded from journals.physiology.org/journal/jappl (073.144.208.122) on April 15, 2022.

Table 2. *Statistical analysis corresponding to the hemodynamic parameters in Table 1*

Heart Rate, beats/min	Pressure, mmHg	Flow Rate, ml/min	Flow Velocity, cm/s	Diameter, mm	Resistance, mmHg·min·ml^{-1}	Re	α
			P value HR				
95	0.851	0.988	0.876	0.825	0.931	0.996	0.497
115	0.820	0.983	0.473	0.731	0.914	0.909	0.139
135	0.123	0.297	0.027	0.559	0.645	0.093	0.007
155	0.003	0.006	<0.001	0.405	0.223	<0.001	<0.001
170	<0.001	<0.001	<0.001	0.484	0.019	<0.001	<0.001
			P value AT				
95		<0.001	0.642	0.088	<0.001	0.005	0.045
115		<0.001	0.337	0.025	<0.001	0.007	0.025
135		<0.001	0.113	0.012	<0.001	0.002	0.011
155		<0.001	0.178	0.008	<0.001	0.002	0.005
170		<0.001	0.218	0.013	<0.001	0.005	0.009
			P value HR × AT				
95		0.999	0.982	0.932	0.992	0.999	0.994
115		0.995	0.978	0.989	0.809	0.891	0.960
135		0.889	0.875	0.964	0.717	0.954	0.852
155		0.959	0.844	0.968	0.226	0.817	0.780
170		0.159	0.989	0.998	0.221	0.712	0.904

P values are given for the effect of heart rate (HR), artery type (AT), and interaction between HR and AT, determined by a two-way ANOVA.

decrease of cardiac output (29, 30), which, in turn, produced a fall in systemic pressure, as shown in Fig. 1*B*. The decrease of pressure led to a decrease of blood flow in peripheral arteries, as shown in Fig. 2, *B*, *E*, and *H*. The recovery of cardiac output and systemic pressure to baseline was mainly caused by an increase of filling pressure and venous pressure stemming from the accumulation of blood in large veins and atrium (29, 30). The increase of systemic pressure (Fig. 1*C*) restored blood flow to baseline, as shown in Fig. 2, *C*, *F*, and *I*. Since heart rates $\leq$ 135 beats/min were in the normal range of physiological regulation, there were negligible changes in pressure and flow waves in peripheral arteries.

The CSA as well as resistance remained relatively unchanged in the peripheral arteries studied as the heart rate increased, which may be caused by the interplay of many factors, such as myogenic, autonomic nervous system, angiotensin II, autacoids, endothelium-based vasoactivity, metabolic massagers, etc. (see details in Ref. 7). Since the vascular resistance mainly resides in the arteriolar bed (5, 10, 11, 15, 16), the changes of arteriolar CSA and major effectors require further investigation.

The rapid pacing altered pressure and flow waveforms, as well as flow velocity profiles in femoral, carotid, and subclavian arteries. The pulse pressure (systolic pressure minus diastolic pressure) and pulse flow (peak flow minus trough flow) decreased during initial and recovery periods after pacing. Systolic pressure and peak flow decreased more significantly at initial pacing than those during the recovery period. There were parabolic velocity profiles of pulsatile blood flow over a cardiac cycle in femoral and carotid arteries, as shown in Fig. 3, *A* and *D*. During the initial period of pacing (heart rates $\geq$ 155 beats/min), these parabolic velocity profiles in trough flow became a velocity profile with fully reversed flow and near-wall retrograde flow in femoral and carotid arteries, respectively (Fig. 3, *B* and *E*), which later returned to parabolic profiles at the recovery period (Fig. 3, *C* and *F*). In the subclavian artery, the velocity profile with near-wall retrograde flow existed during baseline and recovery periods and became a fully reversed velocity profile during the initial period, as shown in Fig. 3, *G–I*. The strong reversal in velocity profiles of these medium-sized peripheral arteries was mainly caused by the abrupt drop of pressure and flow waves at the initial pacing. The increase of heart rate had a small effect on flow velocity profiles during the recovery period because of relatively unchanged time-averaged pressure and flow.

In an in vitro study (9), it was speculated that an increase in Womersley number due to increased heart rate could lead to the near-wall retrograde flow adjacent to the wall and thereby negative WSS over a cardiac cycle. The present study does not support the speculation regarding the frequency of pulsatility, because the increase in Womersley number due to increased heart rate did not increase the incident of flow reversal during the recovery period after pacing, as shown in Fig. 3. Furthermore, many studies have shown that the blood flow becomes less disturbed (more stable) with the increase of Womersley number (8, 24, 25, 27).

Critique of Methods

The present study was limited to a measurement period of 10 min after the onset of rapid atrial pacing. Future studies should focus on chronic effects of recurrent hypotension on the vascular hemodynamics. Furthermore, since the microcirculation is important for understanding syncope and numbness in PSVT, the analysis of pressure and flow waves should be carried out in the distal arterial trees (10, 11, 15, 16). Finally, the curvature and branching pattern were neglected in femoral, carotid, and subclavian arteries. It is known that curvature and side branches lead to disturbed flows, which may stimulate abnormal vasomotor responses (6, 12, 13, 14). A three-dimensional computational fluid dynamic model (12–14), coupled with morphometric data of the peripheral arteries, should be used to investigate the tachycardiac effect on hemodynamics in future studies.

Downloaded from journals.physiology.org/journal/jappl (073.144.208.122) on April 15, 2022.

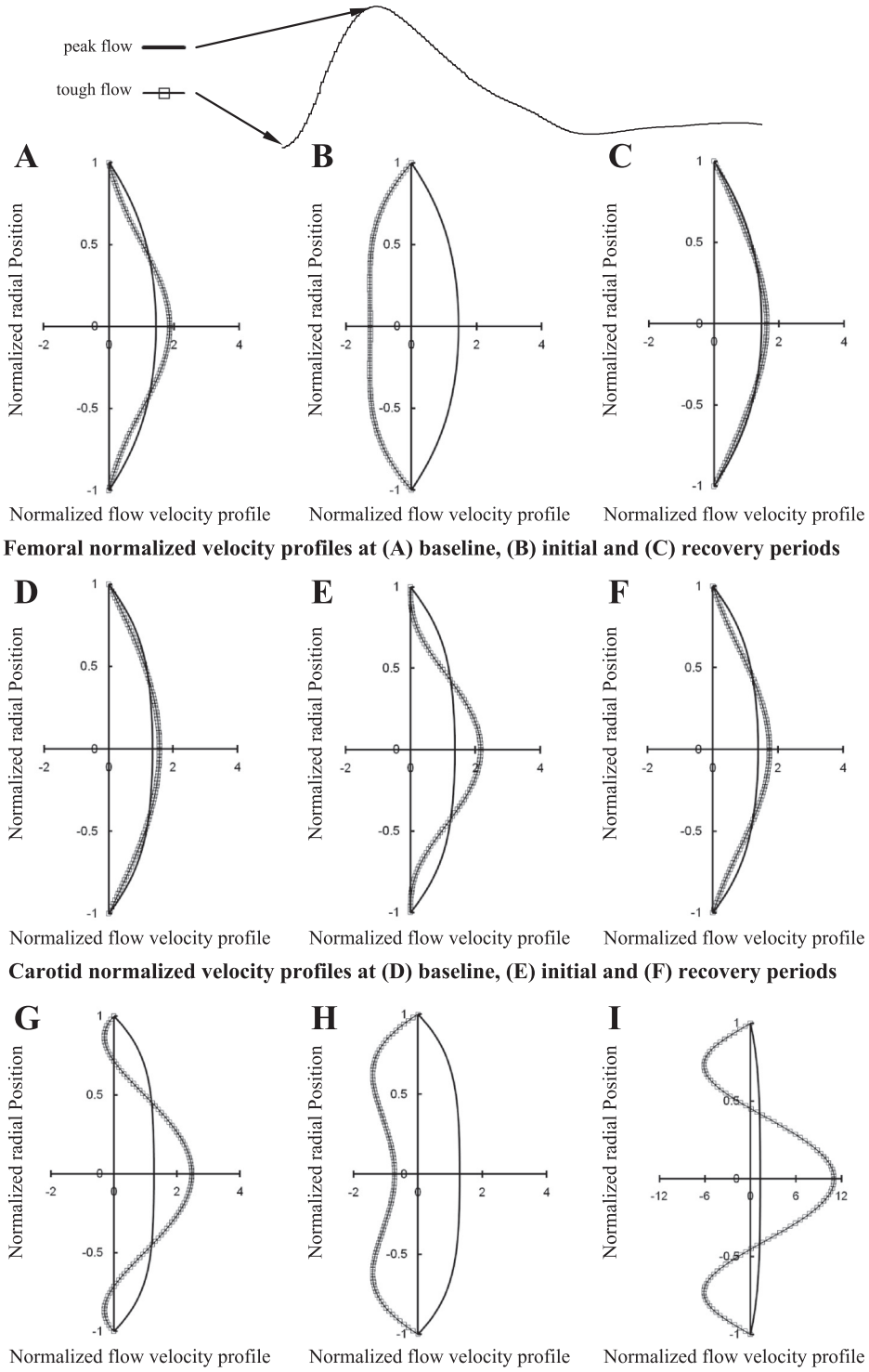

Fig. 3. Normalized flow velocity profile vs. normalized radial position in femoral artery at baseline (~90 beats/min; *A*), initial period (*B*), and recovery period (*C*) after the heart rate of a pig is paced to 155 beats/min, corresponding to Fig. 1, *A–C*. Normalized flow velocity profile is shown vs. normalized radial position in carotid artery (*D–F*) and subclavian artery (*G–I*), in correspondence with *A–C*. Since the actual velocity profile is normalized by the absolute value of its mean flow velocity (averaged over cross-sectional area), the integral of the normalized flow velocity profile is unity. The solid line and the line with markers correspond to the actual velocity profiles that have the maximal and minimal values in a cardiac cycle (peak and trough flows, respectively), as shown in the *top* curve. The radial position is normalized by radius.

Summary and Conclusions

The present study investigated the effects of acute tachycardia on systemic pressure and blood flow of peripheral arteries using experimental measurements and hemodynamic analysis. The pacing-induced hypotension led to a decrease of blood flow in peripheral arteries during the initial period with heart rates $\geq$ 155 beats/min, which altered various hemodynamic parameters (e.g., velocity profile, WSS and OSI, etc.). A stronger reversal existed in velocity profiles and negative WSS at the time instance of trough flow during the initial pacing than at baseline, which resulted in lower time-averaged WSS and higher OSI. The time-averaged WSS typically reflects the shear force acting on the vessel wall averaged over a cardiac

Downloaded from journals.physiology.org/journal/jappl (073.144.208.122) on April 15, 2022.

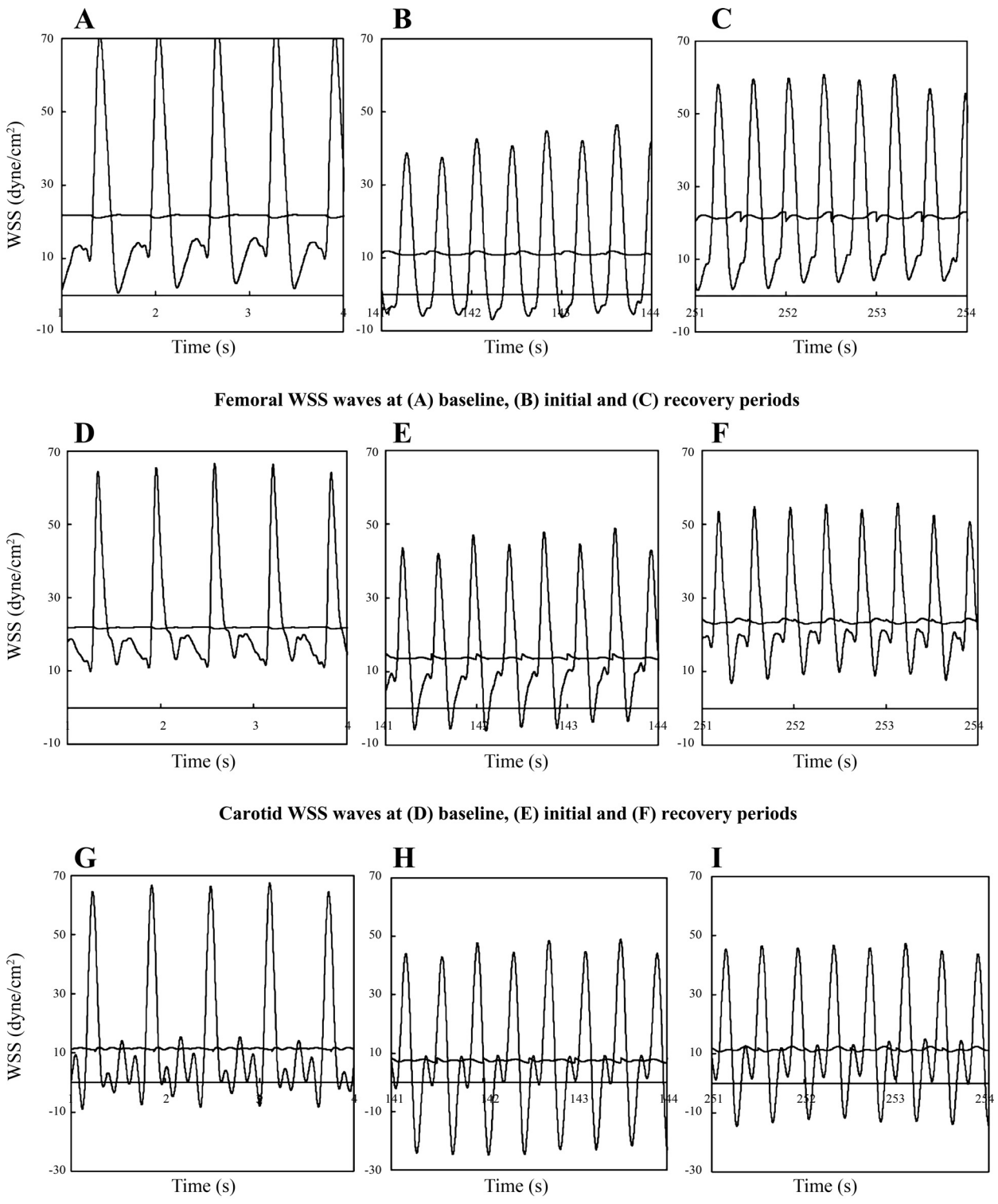

Fig. 4. Wall shear stress (WSS) waves (unit: dynes/cm^2) in femoral artery at baseline (~90 beats/min; *A*), initial period (*B*), and recovery period (*C*) after the heart rate of a pig is paced to 155 beats/min, corresponding to Fig. 1, *A–C*. WSS waves are shown in carotid artery (*D–F*) and subclavian artery (*G–I*), in correspondence with *A–C*. The horizontal solid line represents the time-averaged WSS over a cardiac cycle.

Downloaded from journals.physiology.org/journal/jappl (073.144.208.122) on April 15, 2022.

cycle (8), and OSI describes the magnitude of negative WSS over a cardiac cycle (19). The low time-averaged WSS and high OSI can cause abnormal biological responses in blood vessels (2, 3, 8, 19, 22, 23). This implies that chronic hypotension due to recurrent tachycardia can impair endothelial function, which may contribute to the increased thromboembolic risk due to paroxysmal/chronic atrial fibrillation with high heart rates. Furthermore, an increase in heart rate mainly affects the frequency of pulsatile blood flow during the recovery period of PSVT, while a long-term rapid pacing can result in the tachycardia-induced heart failure and endothelial dysfunction.

APPENDIX

Analytic Solution

When the blood vessel is assumed to be cylindrical, straight, and long, the angular component of blood velocity and all derivatives in the angular direction are zero, so that the continuity and Navier-Stokes equations can be simplified as:

$$\rho\left(\frac{\partial u}{\partial t}+u\frac{\partial u}{\partial x}+v\frac{\partial u}{\partial r}\right)=-\frac{\partial p}{\partial x}+\mu\left(\frac{\partial^2 u}{\partial x^2}+\frac{\partial^2 u}{\partial r^2}+\frac{1}{r}\frac{\partial u}{\partial r}\right) \tag{A1}$$

$$\rho\left(\frac{\partial v}{\partial t}+u\frac{\partial v}{\partial x}+v\frac{\partial v}{\partial r}\right)=-\frac{\partial p}{\partial r}+\mu\left(\frac{\partial^2 v}{\partial x^2}+\frac{\partial^2 v}{\partial r^2}+\frac{1}{r}\frac{\partial v}{\partial r}-\frac{v}{r^2}\right) \tag{A2}$$

where $u(r,x,t)$ and $v(r,x,t)$ are the velocity in axial and radial directions, respectively, $p(x,t)$ is the pressure, and μ and ρ are the dynamic viscosity and density, respectively. When the fully developed flow is considered, v equals zero in a rigid blood vessel. *Equation A1* is simplified to:

$$\rho\left(\frac{\partial u}{\partial t}+u\frac{\partial u}{\partial x}\right)=-\frac{\partial p}{\partial x}+\mu\left(\frac{\partial^2 u}{\partial x^2}+\frac{\partial^2 u}{\partial r^2}+\frac{1}{r}\frac{\partial u}{\partial r}\right) \tag{A3}$$

When only the velocity profile on the CSA of a blood vessel is considered, $\partial u/\partial x$ is assumed to be equal to zero so that *Eq. A3* can be simplified as:

$$\rho\left(\frac{\partial u}{\partial t}\right)=-\frac{\partial p}{\partial x}+\mu\left(\frac{\partial^2 u}{\partial r^2}+\frac{1}{r}\frac{\partial u}{\partial r}\right) \tag{A4}$$

By assuming the blood flow is harmonic and quasi-steady state, the variables are written as:

$$u(r,t)=\mathrm{REAL}\left[\sum_{\omega=0}^{\infty}U(r,\omega)e^{i\omega t}\right]$$
$$p(x,t)=\mathrm{REAL}\left[\sum_{\omega=0}^{\infty}P(x,\omega)e^{i\omega t}\right] \tag{A5}$$

If we substitute *Eq. A5* into *A4*, we obtain:

$$i\omega U+\frac{1}{\rho}\frac{\partial P}{\partial x}=\frac{\mu}{\rho r}\frac{\partial}{\partial r}\left(r\frac{\partial U}{\partial r}\right) \tag{A6}$$

The velocity profile for *Eq. A6* was first obtained by Womersley (31) for pulsatile flow in the form:

$$U=\frac{1}{i\omega\rho}\left(-\frac{\partial P}{\partial x}\right)\left[1-\frac{J_0(\Lambda r/R)}{J_0(\Lambda)}\right] \tag{A7}$$

where $\Lambda^2=i^3\alpha^2$, $\alpha=R\omega\rho/\mu$ is the Womersley number, R is radius of the blood vessel, and J_0 is a Bessel function of zero order and first kind. Integrating the flow velocity over the CSA, we obtain the following equation:

$$-\frac{\partial P}{\partial x}=i\omega\rho Q\Big/\left\{\pi R^2\left[1-\frac{2J_1(\Lambda)}{\Lambda J_0(\Lambda)}\right]\right\} \tag{A8}$$

where $q(x,t)=Q(x,\omega)e^{i\omega t}$ is the volume flow rate determined by experimental measurements, and J_1 is a Bessel function of first order and first kind. Substituting *Eq. A8* into *Eq. A7*, we obtain:

$$U(r,\omega)=\frac{Q(r,\omega)}{\pi R^2}\cdot\left[1-\frac{J_0(\Lambda r/R)}{J_0(\Lambda)}\right]\Big/\left[1-\frac{2J_1(\Lambda)}{\Lambda J_0(\Lambda)}\right] \tag{A9}$$

If $\omega=0$, the steady-state flow has the standard solution as:

$$U(r,0)=2Q(x,0)(R^2-r^2)/\pi R^4 \tag{A10}$$

When *Eqs. A9* and *A10* are substituted into *Eq. A5*, we obtain the following equation:

$$u(r,t)=\mathrm{REAL}\left\{\frac{2Q(x,0)(R^2-r^2)}{\pi R^4}+\sum_{\omega=1}^{\infty}\frac{\frac{Q(r,\omega)}{\pi R^2}\cdot\left[1-\frac{J_0(\Lambda r/R)}{J_0(\Lambda)}\right]}{1-\frac{2J_1(\Lambda)}{\Lambda J_0(\Lambda)}}e^{i\omega t}\right\} \tag{A11}$$

Equation A11 was used to describe the flow velocity profile across the lumen of a blood vessel. Furthermore, WSS follows:

$$\tau(r,t)=\mathrm{REAL}\left[\sum_{\omega=0}^{\infty}T(r,\omega)e^{i\omega t}\right] \tag{A12}$$

and

$$T(r,\omega)=-\frac{\mu Q(r,\omega)}{\pi R^3}\cdot\left[\frac{\Lambda J_1(\Lambda)}{J_0(\Lambda)}\right]\Big/\left[1-\frac{2J_1(\Lambda)}{\Lambda J_0(\Lambda)}\right]\quad\omega\neq 0 \tag{A13}$$

$$T(r,0)=\frac{4\mu}{\pi R^3}Q(r,0)\quad\omega=0 \tag{A14}$$

When *Eqs. A13* and *A14* are substituted into *Eq. A12*, we obtain the following equation:

$$\tau(r,t)=\mathrm{REAL}\left[\frac{4\mu}{\pi R^3}Q(r,0)-\sum_{\omega=1}^{\infty}\frac{\frac{\mu Q(r,\omega)}{\pi R^3}\cdot\frac{\Lambda J_1(\Lambda)}{J_0(\Lambda)}}{1-\frac{2J_1(\Lambda)}{\Lambda J_0(\Lambda)}}e^{i\omega t}\right] \tag{A15}$$

Equation 15 was used to determine WSS on the surface of blood vessel wall.

GRANTS

This research is supported, in part, by National Heart, Lung, and Blood Institute Grant R01 HL-084529 (G. S. Kassab) and American Heart Association Scientist Development Grant 0830181N (Y. Huo).

DISCLOSURES

No conflicts of interest, financial or otherwise, are declared by the author(s).

REFERENCES

1. **Atkins D, Hanusa B, Sefcik T, Apoor W.** Syncope and orthostatic hypotension. *Am J Med* 91: 179–185, 1991.
2. **Bao X, Lu C, Frangos JA.** Mechanism of temporal gradients in shear-induced ERK1/2 activation and proliferation in endothelial cells. *Am J Physiol Heart Circ Physiol* 281: H22–H29, 2001.

Downloaded from journals.physiology.org/journal/jappl (073.144.208.122) on April 15, 2022.

3. **Caro CG, Fitz-Gerald JM, Schroter RC.** Atheroma and arterial wall shear observations. Correlation and proposal of a shear dependent mass transfer mechanism for atherogenesis. *Proc R Soc Lond B Biol Sci* 177: 109–159, 1971.
4. **Chauhan VS, Krahn AD, Klein GJ, Skanes AC, Yee R.** Supraventricular tachycardia. *Med Clin North Am* 85: 193–223, 2001.
5. **Chilian WM.** Microvascular pressures and resistances in the left ventricular subepicardium and subendocardium. *Circ Res* 69: 561–570, 1991.
6. **Debakey ME, Lawrie GM, Glaeser DH.** Patterns of atherosclerosis and their surgical significance. *Ann Surg* 201: 115–131, 1985.
7. **Duncker DJ, Bache RJ.** Regulation of coronary blood flow during exercise. *Physiol Rev* 88: 1009–1086, 2008.
8. **Fung YC.** *Biodynamics: Circulation* (2nd Ed.). New York: Springer-Verlag, 1997.
9. **Gharib M, Beizaie M.** Correlation between negative near-wall shear stress in human aorta and various stages of congestive heart failure. *Ann Biomed Eng* 31: 678–685, 2003.
10. **Huo Y, Kassab GS.** Pulsatile blood flow in the entire coronary arterial tree: theory and experiment. *Am J Physiol Heart Circ Physiol* 291: H1074–H1087, 2006.
11. **Huo Y, Kassab GS.** A hybrid one-dimensional/Womersley model of pulsatile blood flow in the entire coronary arterial tree. *Am J Physiol Heart Circ Physiol* 292: H2623–H2633, 2007.
12. **Huo Y, Wischgoll T, Kassab GS.** Flow patterns in three-dimensional porcine epicardial coronary arterial tree. *Am J Physiol Heart Circ Physiol* 293: H2959–H2970, 2007.
13. **Huo Y, Guo X, Kassab GS.** The flow field along the entire length of mouse aorta, and primary branches. *Ann Biomed Eng* 36: 685–699, 2008.
14. **Huo Y, Choy JS, Svendsen M, Sinha AK, Kassab GS.** Effect of vessel compliance on flow pattern in porcine epicardial right coronary arterial tree. *J Biomech* 42: 594–602, 2009.
15. **Huo Y, Kaimovitz B, Lanir Y, Wischgoll T, Hoffman JI, Kassab GS.** Biophysical model of the spatial heterogeneity of myocardial flow. *Biophys J* 96: 4035–4043, 2009.
16. **Huo Y, Kassab GS.** Effect of compliance and hematocrit on wall shear stress in a model of the entire coronary arterial tree. *J Appl Physiol* 107: 500–505, 2009.
17. **Kassab GS, Rider CA, Tang NJ, Fung YC.** Morphometry of pig coronary arterial trees. *Am J Physiol Heart Circ Physiol* 265: H350–H365, 1993.
18. **Kassab GS, Choy JS, Svendsen M, Sinha AK, Alloosh M, Sturek M, Huo Y, Sandusky GE, Hermiller J.** A novel system for the reconstruction of a coronary artery lumen profile in real time: a preclinical validation. *Am J Physiol Heart Circ Physiol* 297: H485–H492, 2009.
19. **Ku DN, Gidden DP, Zarins CK, Glagov S.** Pulsatile flow and atherosclerosis in the human carotid bifurcation. *Arteriosclerosis* 5: 293–302, 1985.
20. **Leitch JW, Klein GJ, Yee R, Leather RA, Kim YH.** Syncope associated with supraventricular tachycardia. An expression of tachycardia rate or vasomotor response? *Circulation* 85: 1064–1071, 1992.
21 **Lima JAC, Weiss JL, Guzmanm PA, Weisfeldt ML, Reid PR, Traill TA.** Incomplete filling and incoordinate contraction as mechanisms of hypotension during ventricular tachycardia in man. *Circulation* 68: 928–938, 1983.
22. **Lu X, Kassab GS.** Nitric oxide is significantly reduced in ex vivo pig arteries during reverse flow because of increased superoxide production. *J Physiol* 561: 575–582, 2004.
23. **Moore JE, Xu C, Glagov S, Zarins GK, Ku DN.** Fluid wall shear stress measurements in a model of the human abdominal aorta: oscillatory behavior and relationship to atherosclerosis. *Atherosclerosis* 110: 225–240, 1994.
24. **Nerem RM, Seed WA.** An in vivo study of aortic flow disturbances. *Cardiovasc Res* 6: 1–14, 1972.
25. **Nichols WW, O'Rourke MF.** *McDonald's Blood Flow in Arteries: Theoretical, Experimental and Clinical Principles* (4th Ed.). New York: Oxford University Press, 1998.
26. **Paul T, Guccione P, Garson A Jr.** Relation of syncope in young patients with Wolff-Parkinson-White syndrome to rapid ventricular response during atrial fibrillation. *Am J Cardiol* 65: 318–321, 1990.
27. **Pedley TJ.** *The Fluid Mechanics of Large Blood Vessels*. New York: Cambridge University Press, 1980.
28. **Pratt JL, Fleisher GR.** Syncope in children and adolescents. *Pediatr Emerg Care* 5: 80–82, 1989.
29. **Waxman MB, Cameron DA.** The reflex effects of tachycardias on autonomic tone. *Ann N Y Acad Sci* 601: 378–393, 1990.
30. **Wegria R, Frank CW, Wang HH, Lammerant J.** The effect of atrial and ventricular tachycardia on cardiac output, coronary blood flow and mean arterial blood pressure. *Circ Res* 6: 624–632, 1958.
31. **Womersley JR.** Oscillatory motion of a viscous liquid in a thin-walled elastic tube. I. The linear approximation for long waves. *Philios Mag* 46: 199–221, 1955.

Downloaded from journals.physiology.org/journal/jappl (073.144.208.122) on April 15, 2022.